Chemical Physics Letters 808 (2022) 140128

Contents lists available at ScienceDirect

Chemical Physics Letters

journal homepage: www.elsevier.com/locate/cplett

Species-specific acid-base characterization of carnosine and homocarnosine using nuclear magnetic resonance

Arash Mirzahosseini [a,b], Mirsadra Molaei [a], Károly Mazák [a,b], Tamás Pálla [a,b], István Köteles [a,b], Nikolett Varró [c,d], István Mándity [c,d], Béla Noszál [a,b,*]

[a] Department of Pharmaceutical Chemistry, Semmelweis University, Budapest, Hungary
[b] Research Group of Drugs of Abuse and Doping Agents, Hungarian Academy of Sciences, Budapest, Hungary
[c] MTA TTK Lendület Artificial Transporter Research Group, Institute of Materials and Environmental Chemistry, Research Center for Natural Sciences, Hungarian Academy of Sciences, Budapest, Hungary
[d] Department of Organic Chemistry, Semmelweis University, Budapest, Hungary

ARTICLE INFO

Keywords:
Carnosine
Homocarnosine
Titration
Imidazole

ABSTRACT

Carnosine and homocarnosine have long been known to be important constituents of the human metabolome, performing pH- and redox homeostasis-related roles. These are the most important imidazole-containing 'small' chemical entities in biological media. In this work these dipeptides were studied by ^{1}H NMR-pH titration under near-physiological conditions. The resulting acid-base properties are quantified in terms of 6 macroscopic and 24 microscopic protonation constants, which show good agreement with previous results. A deeper knowledge in the physicochemical properties of the studied dipeptides may give further insight into the molecular level interpretation of their biosynthesis pathways, and biochemical reactions.

1. Introduction

Histidine-containing dipeptides carry important functions in biological systems [1]. Their biochemical pathways and the underlying reactivity highly depend on their charge and its distribution. The protonation of the amino, imidazole, and carboxylate sites undergo in different pH ranges, and the protonation state of any of these sites significantly modifies not only the proton-binding ability of the other two sites and the charge-distribution over the molecule, but even the carbon-bound proton-releasing kinetics at the imidazole C2 site [2]. Elucidation of the site- and species-specific protonation properties of these compounds is therefore important to thoroughly understand their biochemical behavior.

Carnosine (CAR) (Fig. 1), the better known of these dipeptides found mainly in muscle tissues, tends to perform chelation with Cu(II) ions, although with much less efficiency (65-fold) than L-histidine at neutral pH [3]. Up to 99 % of the CAR is produced within the skeletal muscle cells, where it plays significant roles in homeostasis during anaerobic respiration, including proton buffering [4], increasing Ca^{2+} sensitivity of the contractile units [5] and reduction of oxidative stress biomarkers [6].

Homocarnosine (hCAR) (Fig. 1), the larger analogue occurs mainly in the human brain and can be detected in vivo by using ^{1}H magnetic resonance spectroscopy (MRS) [7]. Its most sensitive in vitro analytical determination method is matrix assisted laser desorption/ionization mass spectrometry imaging (MALDI-MSI) [8]. The exact function of hCAR is not yet explored; however, it has been reported that it reacts with acrolein, one of the most important neurotoxic byproducts of lipid peroxidation associated with Alzheimer's disease [9].

In 1988, J.W. Pan carried out NMR-pH titrations [10] on CAR, reported the chemical shifts, but protonation constants have not been determined. Subsequently, the characterization of protonation equilibria of carnosine was elaborated in several literature reports [11–19]; in the work of Lytkin et al. [20] the literature data on carnosine protonation was put under meta-analysis and determined precisely using calorimetry (the pK values were extrapolated to zero-order ionic strength 2.59, 6.77, 9.37; T = 298.15 K). Recently, Vistoli et al. have determined the ionization constants of the carboxylic acid (pK_{a1}), the imidazole ring (pK_{a2}), and amino group (pK_{a3}), in different dipeptides, such as CAR (2.76, 6.72, 9.32) and hCAR (2.75, 6.79, 9.88) via potentiometric titration in aqueous solutions at 25 °C and 0.15 mol/L ionic strength [21]. It is apparent from the literature data that not enough

* Corresponding author.
E-mail address: noszal.bela@pharma.semmelweis-univ.hu (B. Noszál).

https://doi.org/10.1016/j.cplett.2022.140128
Received 11 July 2022; Received in revised form 11 October 2022; Accepted 13 October 2022
Available online 18 October 2022

emphasis has been placed on the characterization of homocarnosine as well, although in human brain this metabolite has been used as a promising probe for determining various in vivo parameters, including pH [22]. Although macroscopic protonation constants can be largely attributed to the individual basic moieties in these dipeptides, a more detailed characterization of the acid-base parameters is more meaningful under biomimetic conditions (where the participation of any protonation microspecies may be relevant in highly specific biochemical reactions), including not only the macroscopic, but also the microscopic protonation constants. In this work our aim was to determine all the species- and site-specific protonation constants of CAR and hCAR. A ^{1}H NMR-pH titration method was used to monitor the chemical shifts and coupling constants of the carbon-bound protons of the title compounds to determine 6 macroconstants followed by the determination of 24 microconstants, using a combination of NMR-pH titrations and a deduction method, involving auxiliary compounds that mimic the minor microspecies.

2. Materials and methods

2.1. Materials

Carnosine and all auxiliary reagents for the titrations were purchased from Merck and were used without further purification. Deionized water was prepared with a Milli-Q Direct 8 Millipore system.

2.2. Synthetic protocols

2.2.1. Carnosine methyl ester

0.23 g (1 mmol) carnosine was suspended in 20.0 mL methanol. Hydrochloric acid gas was evolved by dropping concentrated sulfuric acid on solid sodium chloride and the gas was bubbled through the mixture. After 5 min the suspension disappeared resulting in a clear solution. The reaction mixture was stirred overnight and then it was evaporated in vacuo to yield a white glassy solid (0.277 g, 100 %).

2.2.2. Homocarnosine and homocarnosine amide

Homocarnosine and homocarnosine amide were synthesized on H-L-His(Trt)-2CT resin (0,56 mmol/g) and TentaGel R RAM resin (0.19 mmol/g), respectively, with Fmoc-chemistry on a Rink amide linker on a 0.1 mmol scale manually. The coupling of histidine was performed as follows: 3 equivalents of Fmoc-protected amino acid, 3 equivalents of the uronium coupling agent O-(7-azabenzotriazol-1-yl)-N,N,N′,N′-tetramethyluronium hexafluorophosphate and 6 equivalents of N,*N*-diisopropylethylamine were used in N,*N*-dimethylformamide (DMF) as a solvent with shaking for 3 h. After the coupling step, the resin was washed 3 times with dichloromethane, once with methanol and 3 times again with dichloromethane. Deprotection was performed with 2 % 1,8-diazabicyclo[5.4.0]undec-7-ene and 2 % piperidine in DMF in two steps, with reaction times of 5 and 15 min. The resin was washed with the same solvents as described previously. The cleavage was performed with trifluoroacetic acid/water/DL-dithiothreitol (DTT)/triisopropylsilane (TIPS) (90:5:2.5:2.5) at 0 °C for 2 h. The cleavage cocktail was evaporated, and the peptide was precipitated with diethyl ether. After the precipitation, the histidine derivatives were dissolved in 10 % acetic acid solution and were lyophilized. As a final purification, the solid residue that remained after lyophilization was digerated with diisopropyl ether. The crystals gained by this step were washed with diisopropyl ether.

2.3. NMR spectroscopy measurements

A Varian Unity Inova DDR spectrometer (599.9 MHz for ^{1}H) with a 5 mm ^{1}H{^{13}C/^{31}P-^{15}N} pulse field gradient triple resonance probehead at 310.15 ± 0.1 K were used to record all the NMR spectra. As a solvent, H_2O:D_2O 95:5 (V/V) was used with ionic strength settled to 0.15 mol/L using KCl. The pH of each solution was determined with a glass electrode calibrated with aqueous NBS standard buffer solutions at the given temperature. For every sample the volume was set to 550 µL and they contained ca. 1 mmol/L DSS (3-(trimethylsilyl)propane-1-sulfonate) as chemical shift reference. A presaturation sequence was used to suppress the H_2O ^{1}H signal; the mean acquisition parameters for ^{1}H measurements were: number of transients = 16, number of points = 65536, acquisition time = 3.33 s, relaxation delay = 1.5 s.

2.4. pH-potentiometric titrations

A 716 DMS Titrino automatic titrator (Metrohm AG, Herisau, Switzerland) with a Metrohm 6.0204.100 combined pH glass electrode was used for the pH-potentiometric titrations, under automatic PC

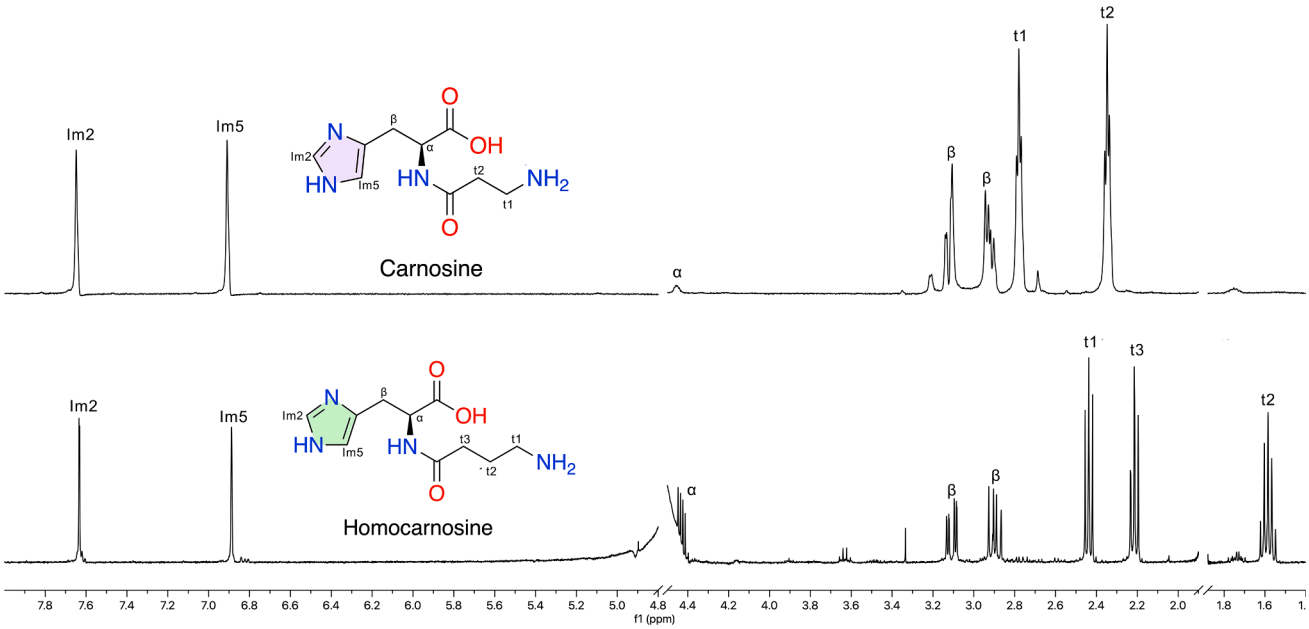

Fig. 1. The constitutional formulas of CAR and hCAR together with their assigned ^{1}H NMR spectra (310.15 K; 5 % D_2O; pH 9.5 and 11.6, respectively).

control. The electrode was calibrated with aqueous NBS standard buffer solutions. Constant temperature (310.15 ± 0.1 K) was provided by a thermostated double-walled glass cell. Difference titrations were carried out in the absence (blank) and presence of ligands. First 1.5 mL of 0.1 mol/L HCl solutions were titrated with 0.1 mol/L NaOH. Constant ionic strength of 0.15 mol/L was provided by the presence of KCl. Next, a ligand was added to the same volume of HCl solution and was subsequently titrated with NaOH. The initial concentration of the ligand was around 5 mmol/L in the titrations. Non-linear parameter fitting provided the protonation constants from the interpolated volume differences.

2.5. Statistical analysis

To analyze the NMR titration data, non-linear regression was performed using R version 4.0.5 (R Foundation for Statistical Computing, Vienna, Austria) with the function:

$$\delta_{obs(pH)} = \frac{\delta_L + \sum_{i=1}^{n} \delta_{H_iL} \bullet 10^{log\beta_i - i \bullet pH}}{\sum_{i=0}^{n} 10^{log\beta_i - i \bullet pH}} \quad (1)$$

where δ_L is the chemical shift of an NMR nucleus in an unprotonated moiety, δ_{H_iL} is the chemical shift of the same NMR nucleus in the i-times protonated species, n is the maximum number of protons that can bind to L, and logβ is the base 10 logarithm of the cumulative protonation macroconstant. The potentiometric titration data were analyzed with the following function:

$$\Delta V_{(pH)} = A \frac{\sum_{i=1}^{n} i \bullet 10^{log\beta_i - i \bullet pH}}{\sum_{i=0}^{n} 10^{log\beta_i - i \bullet pH}} + D \quad (2)$$

where A is the NaOH volume corresponding to one unit of deprotonation, and D is the experimental correction fitting factor. The standard deviations of logβ values from the regression analyses were used to calculate the Gaussian propagation of uncertainty to the other equilibrium constants derived in the Results.

3. Results

3.1. Microspeciation of carnosine

First, carnosine was titrated with potentiometric and NMR methods (Fig. 2) to obtain the macroscopic protonation constants; the constants from both methods were in good agreement with each other and the mean values ± standard errors are listed in Table 1. Next, the UV-pH titration of carnosine was attempted to obtain selective data concerning the imidazole ring, however due to the weak nature of this chromophore (Fig. 2) and a small UV response upon protonation this

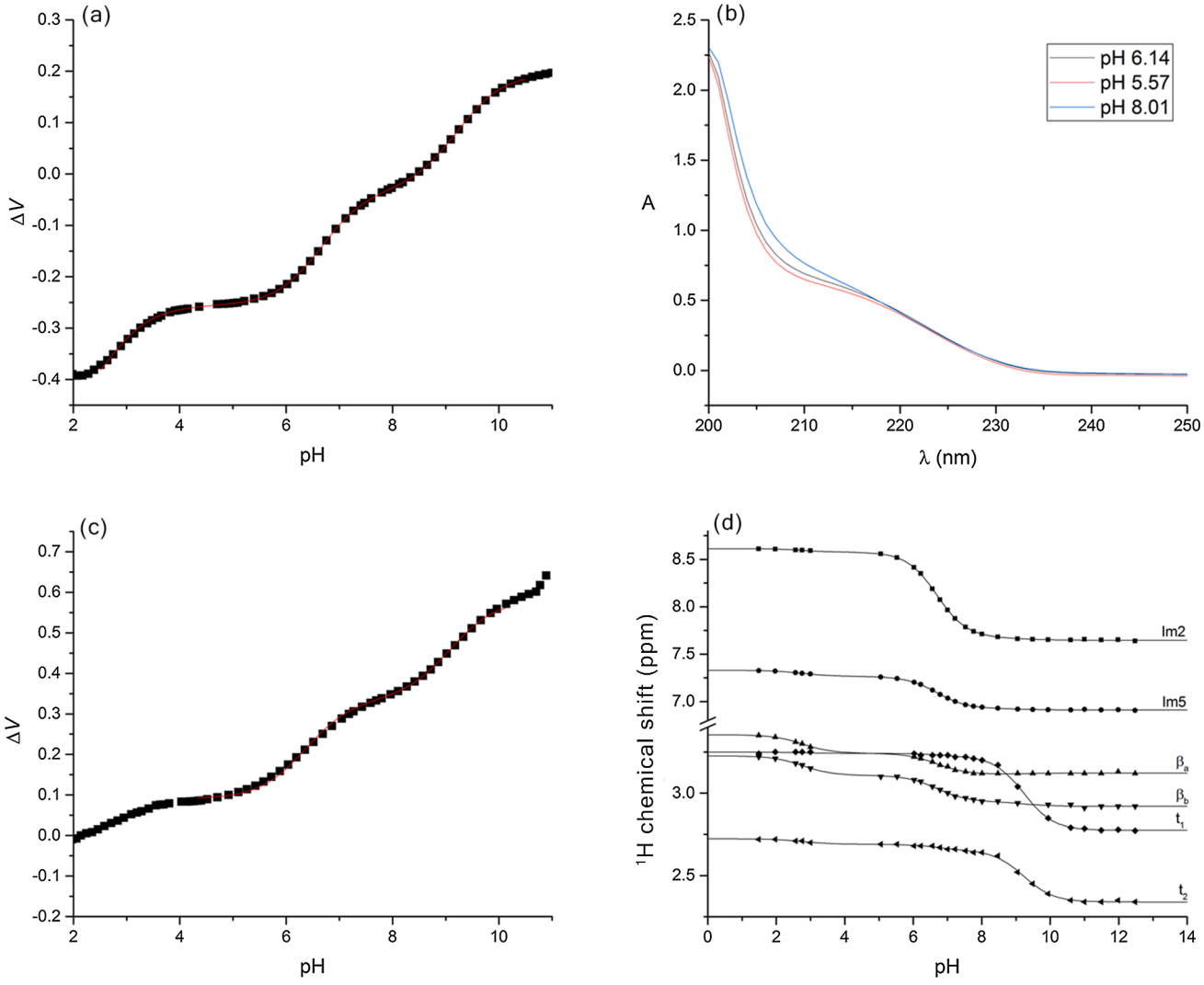

Fig. 2. Top left, the pH-potentiometric titration curve of carnosine; top right, the pH dependent UV spectra of carnosine; bottom left, the pH-potentiometric titration curve of carnosine methyl ester; bottom right, the NMR-pH titration curves of those carnosine ^{1}H signals that had clear visibility in the spectra.

Table 1
The macroscopic protonation constants of carnosine and carnosine methyl ester together with the microscopic protonation constants of carnosine determined at 310 K and 0.15 mol/L ionic strength.

	Macroscopic protonation constants						
	Carnosine				Carnosine methyl ester		
$\log K_1$	9.20 ± 0.08				9.09 ± 0.02		
$\log K_2$	6.69 ± 0.01				6.36 ± 0.02		
$\log K_3$	2.76 ± 0.01						
	Species-specific (microscopic) protonation constants of carnosine						
$\log k^{N}$	9.20 ± 0.08	$\log k^{N}_{Im}$	9.20 ± 0.08	$\log k^{N}_{O}$	9.09 ± 0.02	$\log k^{N}_{ImO}$	9.09 ± 0.02
$\log k^{Im}$	6.69 ± 0.01	$\log k^{Im}_{N}$	6.69 ± 0.01	$\log k^{Im}_{O}$	6.36 ± 0.02	$\log k^{Im}_{NO}$	6.36 ± 0.02
$\log k^{O}$	3.20 ± 0.09	$\log k^{O}_{N}$	3.09 ± 0.02	$\log k^{O}_{Im}$	2.87 ± 0.08	$\log k^{O}_{NIm}$	2.76 ± 0.01

titration afforded no meaningful information. The macroscopic protonation constants (K) are in relation to the microscopic protonation constants (k) (see Fig. 3 for the protonation schemes) as follows:

$$K_1 = k^N + k^{Im} + k^O \tag{3}$$

$$K_2 = k^N \bullet k^{Im}_N + k^N \bullet k^O_N + k^{Im} \bullet k^O_{Im} = \cdots \tag{4}$$

$$K_3 = k^N \bullet k^{Im}_N \bullet k^O_{ImN} = \cdots \tag{5}$$

Concentrations of the various macrospecies comprise the sum of the concentration of those microspecies that contain the same number of protons. For example:

$$[CAR^-] = [N, Im, O^-] \tag{6}$$

$$[HCAR] = [NH^+, Im, O^-] + [N, ImH^+, O^-] + [N, Im, OH] \tag{7}$$

Some samples of macro- and microequilibrium constants are:

$$K_1K_2 = \beta_2 = \frac{[H_2CAR^+]}{[CAR^-] \bullet [H^+]^2} \tag{8}$$

$$k^N = \frac{[NH^+, Im, O^-]}{[N, Im, O^-] \bullet [H^+]} \tag{9}$$

In order to obtain microscopic protonation constants we synthetized and titrated the methyl ester derivative of carnosine, which closely resembles the electron-withdrawing and –sending effects of those microspecies of carnosine (Fig. 3) where the carboxylate moiety is in protonated form. Following the potentiometric titration of carnosine methyl ester the macroscopic protonation constants of this compound were equated with the $\log k^N_O$ and $\log k^{Im}_O$ microconstants of the carnosine microspeciation scheme. Since the macroscopic protonation constants of carnosine itself are also at least 2.5 log units apart, these protonation steps can also be considered to happen almost entirely on a single basic moiety; therefore the macroscopic protonation constants of carnosine were further equated with the $\log k^N$, $\log k^{Im}_N$, and $\log k^O_{ImN}$ microconstants of the carnosine microspeciation scheme. From these five microconstants we could determine the interactivity parameters $\log\Delta E_{N/O} = 0.11 \pm 0.08$ and $\log\Delta E_{Im/O} = 0.33 \pm 0.02$. The interactivity parameter measures how much the protonation constant of a basic moiety is affected by the protonation state of one of its neighboring basic moieties, and vice versa. For example:

$$\log\Delta E_{N/O} = \log k^N - \log k^N_O = \log k^O - \log k^O_N \tag{10}$$

The third and final interactivity parameter, $\log\Delta E_{N/Im}$, was set to 0, since it was evident from the ^{1}H NMR-pH titration data of the imidazole signals that these nuclei practically do not change at all in response to the protonation of the amino group, therefore it can be well assumed that there is no observable interaction between the amino and imidazole moieties. With the three interactivity parameters the remaining microconstants could be calculated, since the interactivity parameter is widely regarded as an invariant parameter between two moieties, regardless of the protonation state of other moieties not considered in the interaction [23], and are listed in Table 1.

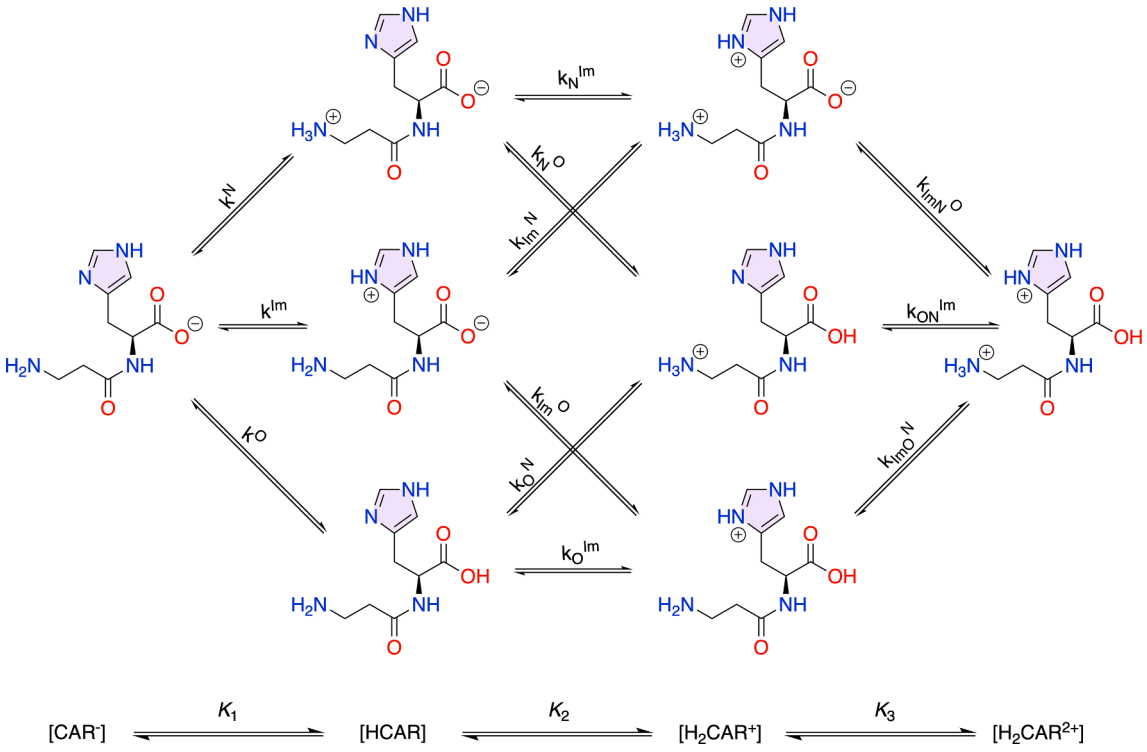

Fig. 3. The protonation scheme of carnosine in terms of stepwise macroscopic protonation constants (K_1, K_2, K_3, bottom line) and the site-specific protonation constants (k^N, k^{Im}, …); N, Im and O denote the amino, imidazole, and carboxylate group, respectively. The protonation scheme of homocarnosine is identical.

3.2. Homocarnosine microspeciation

Homocarnosine titrated using the same methods as for carnosine; the NMR titration curves are depicted in Fig. 4. In this case the model compound of homocarnosine amide was used, instead of the ester, since the amide was easily afforded by the solid-phase peptide synthesis, and amides equally well mimic the electron-withdrawing effects of the protonated carboxylate (COOH) groups [24,25]. Using the same methodology as above the microconstants of homocarnosine were afforded and are listed in Table 2. The interactivity parameters are $\log\Delta E_{N/O} = 0.09 \pm 0.04$ and $\log\Delta E_{Im/O} = 0.31 \pm 0.04$; the third interactivity parameter, $\log\Delta E_{N/Im}$, was again set to 0.

4. Discussion

In this work the protonation constants of carnosine and homocarnosine were determined under near-physiological conditions using ^{1}H NMR and potentiometric titrations, complemented with deductive methods. Usually, with these methods the observed macroscopic protonation constants characterize protonation processes at a molecular level, pertaining to the protonation macrospecies, where only the number of bound protons is known, not the location. However, in the case of carnosine and homocarnosine, the successive macroscopic protonation constant values are all at least 2.5 log units apart, making K_1, K_2, and K_3 macroscopic protonation constants practically identical with the respective major k^N, k^{Im}_N, and k^O_{ImN} microconstants. The successive major protonation steps of the amino, imidazole, and carboxylate moieties show a high degree of similarity between the two compounds as expected, except for the slightly higher amino intrinsic basicity ($\log k^N$) in hCAR due to the stronger electron-donating nature of the longer alkyl chain attached to the amino. The observed protonation shifts in both compounds reflect the structural relationships that are apparent from the formulas. The insensitivity of the imidazole 2 and 5 hydrogens to the amino protonation region (pH range 9–11) is a clear-cut proof of the lack of any significant interaction between the amino and imidazole moieties. This is true both in carnosine and homocarnosine, and is the result of sufficiently large covalent distance between the amino and imidazole moieties, and evidently lack of sufficient flexibility of the compounds to bring these moieties into spatial proximity. The other two interactivity parameters were determined by using a model compound to mimic the protonated carboxylate moiety in minor microspecies (see the relative abundance of microspecies of carnosine in Fig. 5).

It is apparent from the distribution of protonation microspecies in Fig. 5, that in the common physiological pH range of 6 – 8, the most abundant microspecies of both carnosine and homocarnosine (accounting for 90+ % of the microspecies in total) are those of {NH^+, Im, O^-} and {NH^+, ImH^+, O^-}. This is in accordance with the proposed pH buffer role of these dipeptides[4] and is an important factor to consider in the biosynthesis and protein binding of these dipeptide. Carnosine and homocarnosine are synthesized by carnosine synthase, an ATP-grasp with a catalytically active C-terminal [26]. Carnosine synthase has a much higher specificity to histidine than to N-π-methylhistidine or N-τ-methylhistidine [27] (even though they have very similar protonation constants to that of histidine [28]), revealing the importance of the imidazole ring in the substrate-enzyme binding.

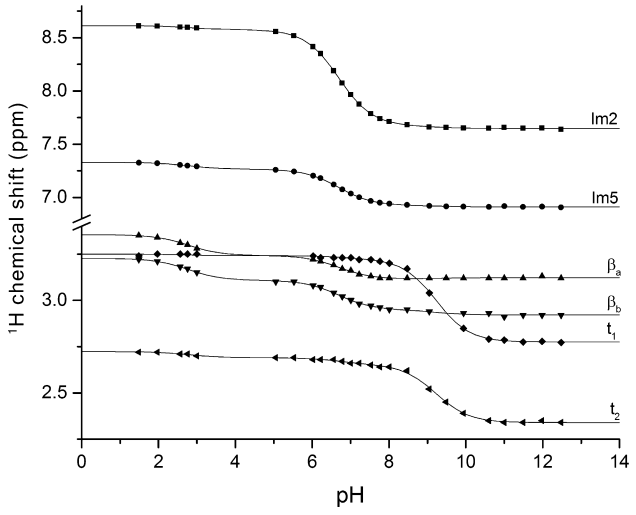

Fig. 4. The NMR-pH titration curves of select homocarnosine ^{1}H signals that had clear visibility in the spectra.

Table 2
The macroscopic protonation constants of homocarnosine and homocarnosine amide together with the microscopic protonation constants of homocarnosine determined at 310 K and 0.15 mol/L ionic strength.

	Macroscopic protonation constants						
	Homocarnosine			Homocarnosine amide			
$\log K_1$	9.91 ± 0.02			9.82 ± 0.04			
$\log K_2$	6.64 ± 0.02			6.33 ± 0.03			
$\log K_3$	2.78 ± 0.09						
	Species-specific (microscopic) protonation constants of homocarnosine						
$\log k^N$	9.91 ± 0.02	$\log k^N_{Im}$	9.91 ± 0.06	$\log k^N_O$	9.82 ± 0.04	$\log k^N_{ImO}$	9.82 ± 0.04
$\log k^{Im}$	6.64 ± 0.02	$\log k^{Im}_N$	6.64 ± 0.02	$\log k^{Im}_O$	6.33 ± 0.03	$\log k^{Im}_{NO}$	6.33 ± 0.03
$\log k^O$	3.18 ± 0.11	$\log k^O_N$	3.09 ± 0.1	$\log k^O_{Im}$	2.87 ± 0.1	$\log k^O_{NIm}$	2.78 ± 0.09

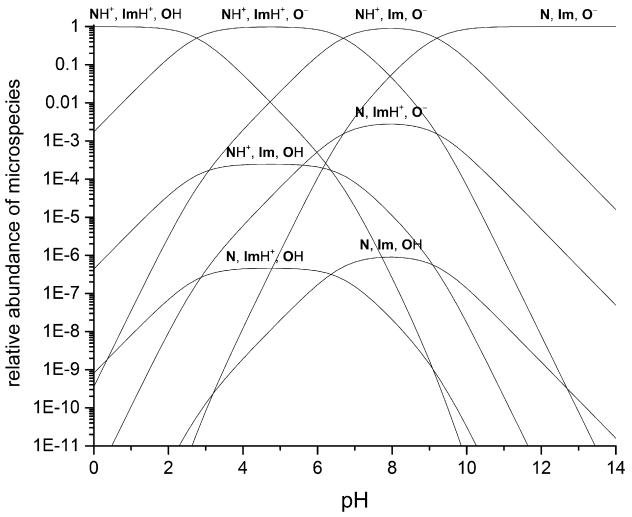

Fig. 5. The relative concentrations (in logarithmic scale) of the various microspecies of carnosine are depicted in a pH-dependent distribution diagram.

Funding

The research was financed by the Higher Education Institutional Excellence Programme of the Ministry of Human Capacities in Hungary, within the framework of the molecular biology thematic programme of Semmelweis University (TKP2021-EGA-24), and the ÚNKP-21-5-SE-4 New National Excellence Program of the Hungarian Ministry for Innovation and Technology from the source of the National Research, Development and Innovation Fund.

The Lendület grant from the Hungarian Academy of Sciences is gratefully acknowledged. This work was completed in the ELTE Thematic Excellence Programme supported by the Hungarian Ministry for Innovation and Technology. Project no. 2018-1.2.1-NKP-2018-00005 has been implemented with the support provided from the National

Research, Development and Innovation Fund of Hungary, financed under the 2018-1.2.1-NKP funding scheme.

Arash Mirzahosseini is grateful for the János Bolyai Research Scholarship of the Hungarian Academy of Sciences. The funders had no role in study design, data collection and analysis, decision to publish, or preparation of the manuscript.

CRediT authorship contribution statement

Arash Mirzahosseini: Conceptualization, Methodology, Formal analysis, Investigation, Writing – original draft, Visualization, Funding acquisition. **Mirsadra Molaei:** Investigation, Writing – original draft, Visualization. **Károly Mazák:** Investigation. **Tamás Pálla:** Formal analysis. **István Köteles:** Investigation. **Nikolett Varró:** Investigation. **István Mándity:** Methodology, Resources, Funding acquisition. **Béla Noszál:** Conceptualization, Resources, Writing – review & editing, Supervision, Funding acquisition.

Declaration of Competing Interest

The authors declare that they have no known competing financial interests or personal relationships that could have appeared to influence the work reported in this paper.

Data availability

Data will be made available on request.

References

[1] M.E. Brosnan, J.T. Brosnan, Histidine metabolism and function, J. Nutr. 150 (2020) 2570S–2575S.
[2] B. Noszal, D.L. Rabenstein, Nitrogen-protonation microequilibria and C(2)-deprotonation microkinetics of histidine, histamine, and related compounds, J. Phys. Chem. 95 (1991) 4761–4765.
[3] S. Velez, N.G. Nair, V.P. Reddy, Transition metal ion binding studies of carnosine and histidine: biologically relevant antioxidants, Colloids Surf. B Biointerfaces 66 (2) (2008) 291–294.
[4] A.A. Boldyrev, G. Aldini, W. Derave, Physiology and pathophysiology of carnosine, Physiol. Rev. 93 (2013) 1803–1845.
[5] T.L. Dutka, C.R. Lamboley, M.J. McKenna, R.M. Murphy, G.D. Lamb, Effects of carnosine on contractile apparatus Ca2+ sensitivity and sarcoplasmic reticulum Ca2+ release in human skeletal muscle fibers, J. Appl. Physiol. 112 (2012) 728–736.
[6] M.-F. Palin, J. Lapointe, C. Gariépy, D. Beaudry, C. Kalbe, M. Kanzaki, Characterisation of intracellular molecular mechanisms modulated by carnosine in porcine myoblasts under basal and oxidative stress conditions, PLOS ONE 15 (9) (2020) e0239496.
[7] O.A.C. Petroff, R.H. Mattson, K.L. Behar, F. Hyder, D.L. Rothman, Vigabatrin increases human brain homocarnosine and improves seizure control, Ann. Neurol. 44 (1998) 948–952.
[8] T. Vallianatou, et al., Integration of mass spectrometry imaging and machine learning visualizes region-specific age-induced and drug-target metabolic perturbations in the brain, ACS Chem. Neurosci. 12 (2021) 1811–1823.
[9] M. Carini, G. Aldini, G. Beretta, E. Arlandini, R.M. Facino, Acrolein-sequestering ability of endogenous dipeptides: characterization of carnosine and homocarnosine/acrolein adducts by electrospray ionization tandem mass spectrometry, J. Mass Spectrom. 38 (2003) 996–1006.
[10] J.W. Pan, J.R. Hamm, D.L. Rothman, R.G. Shulman, Intracellular pH in human skeletal muscle by 1H NMR, Proc. Natl. Acad. Sci. 85 (1988) 7836–7839.
[11] E.M. Moustafa, M. Korany, N.A. Mohamed, T. Shoeib, Carnosine complexes and binding energies to some biologically relevant metals and platinum containing anticancer drugs, Inorganica Chim. Acta 421 (2014) 123–135.
[12] R.P. Bonomo, V. Bruno, E. Conte, G. De Guidi, D.L. Mendola, G. Maccarrone, F. Nicoletti, E. Rizzarelli, S. Sortino, G. Vecchio, Potentiometric, spectroscopic and antioxidant activity studies of SOD mimics containing carnosine, Dalton Trans. (23) (2003) 4406–4415.
[13] P.G. Daniele, E. Prenesti, G. Ostacoli, Ultraviolet–circular dichroism spectra for structural analysis of copper(II) complexes with aliphatic and aromatic ligands in aqueous solution, J. Chem. Soc. Dalton Trans. 3269–3275 (1996), https://doi.org/10.1039/DT9960003269.
[14] T. Gajda, B. Henry, J.-J. Delpuech, Multinuclear NMR and potentiometric study on tautomerism during protonation and zinc(II) complex formation of some imidazole-containing peptide derivatives, J. Chem. Soc. Perkin Trans. 2 (1994) 157–164, https://doi.org/10.1039/P29940000157.
[15] E. Gaggelli, G. Valensin, 1H and 13C NMR relaxation investigation of the calcium complex of β-alanyl-L-histidine (carnosine) in aqueous solution, J. Chem. Soc. Perkin Trans. 2 (1990) 401–406, https://doi.org/10.1039/P29900000401.
[16] E. Farkas, I. Sóvágó, A. Gergely, Studies on transition-metal–peptide complexes. Part 8. Parent and mixed-ligand complexes of histidine-containing dipeptides, J. Chem. Soc., Dalton Trans. (8) (1983) 1545–1551.
[17] P.G. Daniele, P. Amico, G. Ostacoli, Heterobinuclear Cu(II) L-carnosine complexes with Cd(II) or Zn(II) in aqueous solution, Inorganica Chim. Acta 66 (1982) 65–70.
[18] P.G. Daniele, E. Prenesti, V. Zelano, G. Ostacoli, Chemical relevance of the copper (II)—l-carnosine system in aqueous solution: A thermodynamic and spectrophotometric study, Spectrochim. Acta Part Mol. Spectrosc. 49 (1993) 1299–1306.
[19] C. Abate, et al., Understanding the behaviour of carnosine in aqueous solution: an experimental and quantum-based computational investigation on acid–base properties and complexation mechanisms with Ca2+ and Mg2+, New J. Chem. 45 (2021) 20352–20364.
[20] A.I. Lytkin, V.P. Barannikov, V.G. Badelin, O.N. Krutova, Enthalpies of acid dissociation of l-carnosine in aqueous solution, J. Therm. Anal. Calorim. 139 (2020) 3683–3689.
[21] G. Vistoli, V. Straniero, A. Pedretti, L. Fumagalli, C. Bolchi, M. Pallavicini, E. Valoti, B. Testa, Predicting the physicochemical profile of diastereoisomeric histidine-containing dipeptides by property space analysis: Physicochemical profile of diastereoisomeric peptides, Chirality 24 (7) (2012) 566–576.
[22] D.L. Rothman, K.L. Behar, J.W. Prichard, O.A.C. Petroff, Homocarnosine and the measurement of neuronal pH in patients with epilepsy, Magn. Reson. Med. 38 (1997) 924–929.
[23] M.A. Santos, M.A. Esteves, M.C. Vaz, J.J.R. Fraústo da Silva, B. Noszal, E. Farkas, Microscopic acid–base equilibria of a synthetic hydroxamate siderophore analog, piperazine-1,4-bis(N-methylacetohydroxamic acid), J Chem Soc Perkin Trans (10) (1997) 1977–1983.
[24] B. Noszal, P. Sandor, Rota-microspeciation of aspartic acid and asparagine, Anal. Chem. 61 (1989) 2631–2637.
[25] K. Mazák, B. Noszál, Advances in microspeciation of drugs and biomolecules: species-specific concentrations, acid-base properties and related parameters, J. Pharm. Biomed. Anal. 130 (2016) 390–403.
[26] S. Kwiatkowski, A. Kiersztan, J. Drozak, Biosynthesis of carnosine and related dipeptides in vertebrates, Curr. Protein Pept. Sci. 19 (8) (2018) 771–789.
[27] J. Drozak, M. Veiga-da-Cunha, D. Vertommen, V. Stroobant, E. Van Schaftingen, Molecular identification of carnosine synthase as ATP-grasp domain-containing protein 1 (ATPGD1), J. Biol. Chem. 285 (2010) 9346–9356.
[28] M. Tanokura, 1H-NMR study on the tautomerism of the imidazole ring of histidine residues. I. Microscopic pK values and molar ratios of tautomers in histidine-containing peptides, Biochim. Biophys. Acta 742 (1983) 576–585.